Oxygen vacancy formation and migration in Sr- and Mg-doped $LaGaO_3$: a density functional theory study*

Zhang Jie(张 洁), Liang Er-Jun(梁二军)†, Sun Qiang(孙 强), and Jia Yu(贾 瑜)

School of Physics and Engineering, Zhengzhou University, Zhengzhou 450052, *China*

(Received 28 September 2011; revised manuscript received 17 October 2011)

Oxygen vacancy formation and migration in $La_{0.9}Sr_{0.1}Ga_{0.8}Mg_{0.2}O_{3-\delta}$ (LSGM) with various crystal symmetries (cubic, rhombohedral, orthorhombic, and monoclinic) are studied by employing first-principles calculations based on density functional theory (DFT). It is shown that the cubic LSGM has the smallest band gap, oxygen vacancy formation energy, and migration barrier, while the other three structures give rise to much larger values for these quantities, implying the best oxygen ion conductivity of the cubic LSGM among the four crystal structures. In our calculations, one oxygen vacancy migration pathway is considered in the cubic and rhombohedral structures due to all the oxygen sites being equivalent in them, while two vacancy migration pathways with different migration barriers are found in the orthorhombic and monoclinic symmetries owing to the existence of nonequivalent O_1 and O_2 oxygen sites. The migration energies along the migration pathway linking the two O_2 sites are obviously lower than those along the pathway linking the O_1 and O_2 sites. Considering the phase transitions at high temperatures, the results obtained in this paper can not only explain the experimentally observed different behaviours of the oxygen ionic conductivity of LSGM with different symmetries, but also predict the rational crystal structures of LSGM for solid oxide fuel cell applications.

Keywords: density functional theory, oxygen vacancy formation energy, oxygen vacancy migration energy, migration pathway

PACS: 72.60.+g, 71.20.Ps, 72.10.Fk **DOI:** 10.1088/1674-1056/21/4/047201

1. Introduction

Fast oxygen ion conductors are important materials because of their prospective applications in oxygen pumps, oxygen sensors, and solid oxide fuel cells (SOFCs). It has been widely noted that many perovskite-type oxides exhibit high diffusivity of oxygen ions.[1−3] Recently, Sr- and Mg-doped $LaGaO_3$ has attracted extensive attention owing to its higher oxygen ionic conductivity than the standard oxygen ionic conductor yttria-stabilized zirconia, and its stability in a wide range of oxygen partial pressures.[4−6] It is expected to be one of the best candidates as a solid electrolyte in SOFCs. The incorporation of Sr and Mg dopants with lower density to form the system $La_{0.9}Sr_{0.1}Ga_{0.8}Mg_{0.2}O_{3-\delta}$ (denoted as LSGM) gives rise to the highly mobile oxygen vacancies that are responsible for the observed ionic conductivity. Following the initial discovery by Ishihara *et al.*[4,5] numerous experiments have been carried out on the $LaGaO_3$-based materials to investigate the oxygen ion conductivity,[7,8] structural properties,[9−12] electrolyte performance within the SOFCs,[13,14] and the effect of transition-metal doping.[15,16]

An electrolyte material for the SOFC application requires an electronic conductivity as low as possible and an oxygen ionic conductivity as high as possible. The ionic conductivity is controlled by the formation and migration energies of oxygen vacancies, which are closely related to its crystal structures. However, the crystal structure of LSGM has been reported to be cubic,[17,18] orthorhombic,[9,10] and monoclinic[11,12] at room temperature (RT). Feng[17] and Trofimenko[18] declared a cubic structure with space group $Pm\bar{3}m$ (No. 221) for LSGM at room temperature; Lerch *et al.*[10] carried out powder neutron diffraction measurements and concluded that the crystal structure of LSGM was orthorhombic with space group *Imma* (No. 74) at room temperature and cubic with space group $Pm\bar{3}m$ (No. 221) at 1073 K, respectively. More complicated structural changes in LSGM have been detected by Slater,[11] who claimed that

*Project supported by the National Natural Science Foundation of China (Grant No. 10974183).

†Corresponding author. E-mail: ejliang@zzu.edu.cn

© 2012 Chinese Physical Society and IOP Publishing Ltd

$La_{0.9}Sr_{0.1}Ga_{0.8}Mg_{0.2}O_{3-\delta}$ has a monoclinic structure with space group $I2/a$ (No. 15) at room temperature, and two-phase transitions appear between 723 K and 1273 K: monoclinic (pseudo-OR)–monoclinic (pseudo-Rh)–rhombohedral ($R3c$). These very contradictory reports on the crystal structure of LSGM might result from the fact that LSGM adopts a perovskite-type structure with extremely weak deformations from the cubic aristotype, and that it is very difficult to distinguish among different kinds of slightly distorted structures by the used methods, or that cubic, monoclinic and orthorhombic are all possibly the room-temperature crystal structures for LSGM, depending on its synthesizing method and the conditions used by the different groups. However, these problems have not yet been solved for this solid solution and no decisive conclusion can be drawn. The uncertainty makes it difficult to elucidate the intrinsic relationship between the ionic conductivity and the crystal structures.

In a previous paper, we reported the synthesis and electrical properties of $La_{0.9}Sr_{0.1}Ga_{0.8}Mg_{0.2}O_{3-\delta}$ by low- and high-temperature solid state reactions (SSR1 and SSR2) and laser rapid solidification (LRS).[8] It was shown that they exhibited very different ionic conductivity with temperature. The LSGM prepared by laser rapid solidification exhibited a drastic enhancement in ionic conductivity at high temperatures with respect to that prepared by a high-temperature solid state reaction (SSR2), though both are pure and have similar relative densities. Raman spectroscopic studies of these samples suggested strongly that they crystallized in different structures.[19] Why the sample prepared by laser rapid solidification presents unique electrical properties remains an interesting problem to be explored.

First-principles calculations are an important tool for the detailed understanding of the transport mechanisms of the electrons and oxygen vacancies.[20−34] Many computational simulations have been conducted to investigate the defect formation energies[20] and oxygen vacancy migration energy[21−23] of $LaGaO_3$-based oxygen ion conductors. These previous works were successful in reproducing some of the trends found by the experiments. In this paper, we systematically study the electronic structures, oxygen vacancy, formation, and migration in cubic, rhombohedral, orthorhombic, and monoclinic LSGM by first-principles calculations. Our aim is to elucidate the mechanisms of ionic conductivity in different crystal structures of the LSGM, and explain the experimentally observed drastic enhancement in ionic conductivity at high LSGM temperatures prepared by LRS with respect to that prepared by high-temperature solid state reaction. Besides, this study may also predict rational crystal structures which are important for experimentalists in synthesizing a high performance LSGM electrolyte for SOFC applications.

2. Calculation methods

We employed the DMol^3 code,[35,36] which is based on density functional theory (DFT). According to the reported results of other similar perovskite materials,[20,30] the exchange and correlation (XC) energy of the electrons are described by the generalized gradient approximation (GGA) with the Perdew–Wang (PW91) functional.[37] DFT semicore pseudopots (DSPPs) were included via a local pseudopotential for all electron calculations, where the effect of core electrons is substituted by a simple potential including some degree of relativistic effects. The virtual crystal approximation (VCA) was employed with small amounts of Sr- and Mg-doping in $LaGaO_3$ (LSGM). The VCA, at least in principle, can be used to investigate and predict the effect of doping, which has already been proven to be accurate for solid solutions of perovskites.[38] The VCA calculations are based on a weighting of the contribution of the pseudopotentials according to the site occupancies.[38] Fractional atomic coordinates and interatomic distances for the different crystal structures of LSGM were used.[10,12] Four symmetries, i.e. cubic (C-LSGM), rhombohedral (R-LSGM), orthorhombic (O-LSGM), and monoclinic (M-LSGM) structures, were considered in the study. The k-point meshes of Brillouin zone sampling in primitive cells, based on the Monkhorst–Pack scheme, were 6×6×6 for C-LSGM (10 irreducible points), 4×4×4 for R-LSGM (32 irreducible points), 4×5×4 for O-LSGM (40 irreducible points), and 4×4×4 for M-LSGM (32 irreducible points) in order to obtain absolute energy convergence (≤ 0.5 meV·atom^{-1}). Lattice constants and internal positions in the primitive cell of each crystal structure were fully optimized under the condition of residual force ≤ 0.1 eV·Å^{-1} (1 Å=0.1 nm).

The supercells, each of which contain an oxygen vacancy, were constructed using the fully optimized primitive cell of C-LSGM, R-LSGM, O-LSGM, and M-LSGM, respectively. They are 2×2×4 for C-LSGM, and 2×2×2 for R-LSGM, O-LSGM, and M-LSGM. Each supercell with an oxygen vacancy has 79 atoms. The k-meshes of 3×3×1 for C-LSGM, 2×3×2

for O-LSGM, and 2×2×2 for R-LSGM and M-LSGM were chosen for attaining absolute energy convergence ($\leq$ 0.5 meV·atom^{-1}). Structural relaxation was limited within a spherical region with a radius of 3.2 Å from a defect site. For the calculation of the total energy of oxygen molecules in the gas phase, an O_2 molecule was put into a vacuum cell whose dimensions were identical to those of the supercell of O-LSGM. The k-mesh was taken to be 2×2×2 (four irreducible points). Spin-polarization was taken into account for the calculation of O_2. The complete linear synchronous transit/quadratic synchronous transit (complete LST/QST) tools in the DMOL^3 code are used,[35,36,39] which also shows the transition state in a simple manner and obtains the barriers for oxygen vacancy migration (E_m) immediately.

3. The structural and electronic properties of perfect LSGM

3.1. The structures of LSGM with various symmetries

Figures 1(a)–1(d) show the schematic structures of the LSGMs with cubic ($pm\bar{3}m$), rhombohedral ($R3c$), orthorhombic ($Imma$), and monoclinic ($I2/a$) symmetries using ball-and-stick primitive cell models, respectively. $Pm\bar{3}m$ is an ideal cubic perovskite structure, while $R3c$, $Imma$, and $I2/a$ contain a network of corner-sharing GaO_6 octahedra and belong to the family of rotationally distorted perovskites.

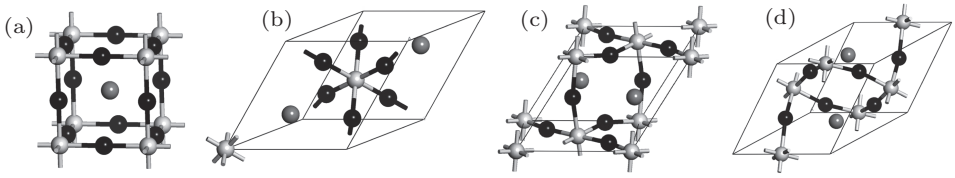


Fig. 1. Ball-and-stick primitive cell models of LSGMs with different crystal symmetries (the grey, white, and black spheres represent La/Sr, Ga/Mg, and O ions, respectively): (a) C-LSGM ($Pm\bar{3}m$); (b) R-LSGM ($R3c$); (c) O-LSGM ($Imma$); (d) M-LSGM ($I2/a$).

Before carrying out vacancy calculations, the crystal structures of LSGMs with various symmetries were simulated using energy minimization procedures. The calculated lattice parameters are listed in Table 1, and the experimental values are also presented for comparison. Our calculated results are in good agreement with the experimental data, providing support for the reliability and validity of the subsequent defect simulations.

Table 1. The calculated and experimental structural parameters and calculated band gaps of cubic, rhombohedral, orthorhombic, and monoclinic LSGM.

LSGM system	Lattice parameter		Band gap/eV
	calc.	expt.	
C-LSGM	$a = 3.9000$ Å	$a = 3.9760$ Å	3.21
	$\alpha = \beta = \gamma = 90°$	$\alpha = \beta = \gamma = 90°$	
R-LSGM	$a = 5.5903$ Å	$a = 5.5592$ Å	3.70
	$c = 13.6776$ Å	$c = 13.4354$ Å	
	$\alpha = \beta = 90°$	$\alpha = \beta = 90°$	
	$\gamma = 120°$	$\gamma = 120°$	
O-LSGM	$a = 5.5085$ Å	$a = 5.5179$ Å	3.62
	$b = 7.7973$ Å	$b = 7.8200$ Å	
	$c = 5.5756$ Å	$c = 5.5394$ Å	
	$\alpha = \beta = \gamma = 90°$	$\alpha = \beta = \gamma = 90°$	
M-LSGM	$a = 7.8135$ Å	$a = 7.8160$ Å	3.51
	$b = 5.5742$ Å	$b = 5.5393$ Å	
	$c = 5.5108$ Å	$c = 5.5147$ Å	
	$\alpha = \gamma = 90°$	$\alpha = \gamma = 90°$	
	$\beta = 90.121°$	$\beta = 90.060°$	

3.2. Electronic properties

The calculated total density of states (TDOSs) of the LSGMs with various symmetries is shown in Fig. 2. They share common features: two valence bands located between −18 eV and −13 eV, and −8 eV and 0 eV, respectively, and the band gaps are larger than 3.0 eV. The calculated band gaps are presented in Table 1. The C-LSGM has the smallest band gap of 3.21 eV, while the band gaps for the R-LSGM, O-LSGM, and M-LSGM are 3.70, 3.62, and 3.51 eV, respectively. These band gap values should be considered as the lowest limit since it is well known that GGA generally underestimate the band gaps of insulators. The large band gaps calculated for various structures imply that LSGMs are poor electronic conductors.

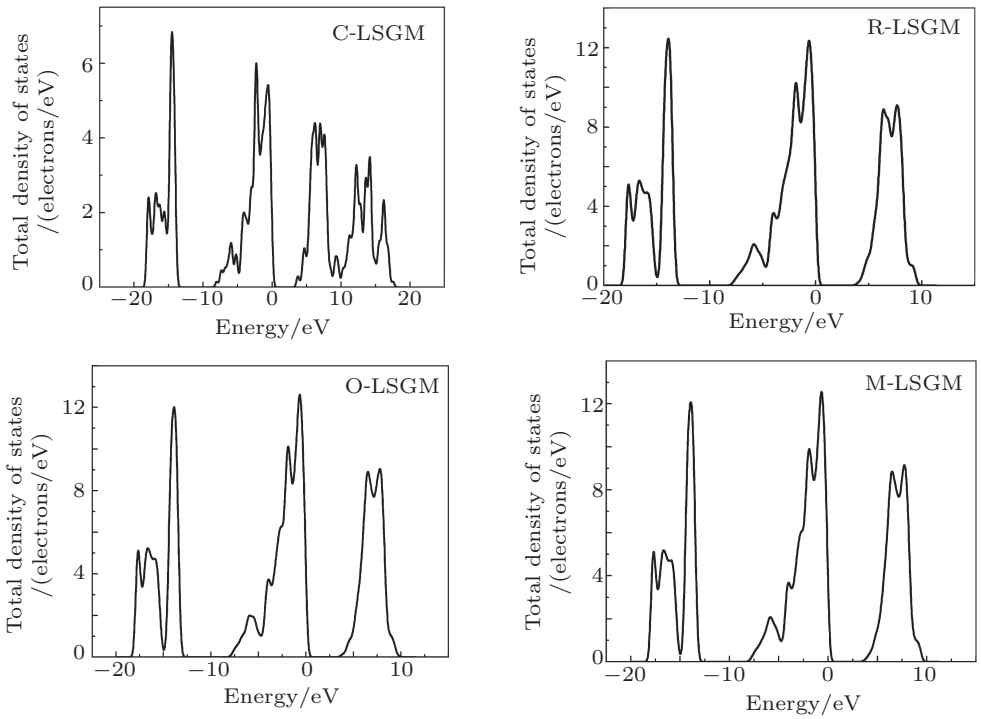


Fig. 2. Calculated total DOS for C-LSGM, R-LSGM, O-LSGM, and M-LSGM.

4. Oxygen vacancy formation and migration

The main transport mechanism in Sr- and Mg-doped $LaGaO_3$ (LSGM) is the migration of oxygen vacancies which are formed in the following defect reactions

$$2\mathrm{SrO}\xrightarrow{\mathrm{La_2O_3}}2\mathrm{Sr'La}+\ddot{V}_{\mathrm{o}}+2\mathrm{Oo}^{\times},$$
$$2\mathrm{MgO}\xrightarrow{\mathrm{Ga_2O_3}}2\mathrm{Mg'Ga}+\ddot{V}_{\mathrm{o}}+2\mathrm{Oo}^{\times}, \quad (1)$$

where $\ddot{V}_{\mathrm{o}}$ represents oxygen vacancy and $O\mathrm{o}^{\times}$ is the oxygen in the crystal lattice. The activation energy normally includes the formation energy and the migration energy of the oxygen vacancies.

The formation energy of an oxygen vacancy was evaluated using the following equation

$$E_{\mathrm{f}}(\ddot{V}_{\mathrm{o}}) = E_{\ddot{V}_{\mathrm{o}}} + \frac{1}{2}E_{\mathrm{O_2}} - E_{\mathrm{perfect}}, \quad (2)$$

where $E_{\ddot{V}_{\mathrm{o}}}$ is the calculated total energy per supercell containing an oxygen vacancy, $\frac{1}{2}E_{\mathrm{O_2}}$ is the calculated energy for an oxygen atom in the molecule and E_{perfect} corresponds to the calculated total energy of the same supercell for the perfect crystal.

The formation energies of an oxygen vacancy with respect to the calculated energy for an oxygen atom in the molecule ($\frac{1}{2}E_{\mathrm{O_2}}$) for the cubic, rhombohedral, orthorhombic, and monoclinic LSGMs were computed and are shown in Fig. 3. Only one vacancy site was studied for the cubic and rhombohedral structures due to all the equivalent oxygen sites in them, while two oxygen vacancy formation energies were calculated for the orthorhombic and monoclinic structures owing to two nonequivalent oxygen sites (named O_1 and O_2, respectively). The oxygen vacancy formation energy for the O_2 site is higher than that for the O_1 site, but the difference is rather small (0.06 eV–0.07 eV). Figure 3 shows that the vacancy formation energy of

the cubic LSGM is 3.96 eV, much lower than those of the rhombohedral, orthorhombic, and monoclinic LSGMs, all of which are about 5.50 eV. This means that the oxygen ions in the C-LSGM may be more easily activated for transportation.

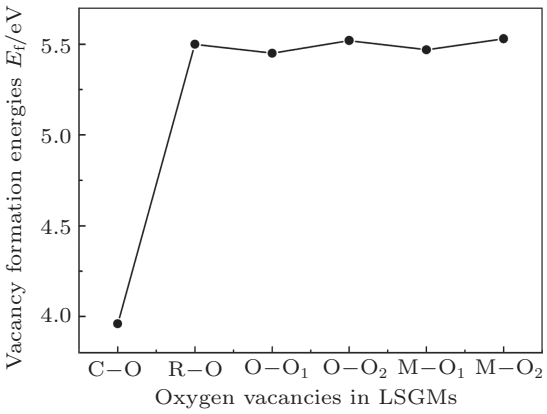


Fig. 3. The calculated vacancy formation energies (E_f) of LSGMs with respect to the calculated energy $(1/2)E_{O_2}$ for an oxygen atom in the molecule. C–O and R–O correspond to the oxygen vacancy in cubic and rhombohedral LSGMs, respectively. O–O_1, O–O_2, M–O_1, and M–O_2 correspond to oxygen vacancies at the O_1 and O_2 site in orthorhombic and monoclinic LSGMs, respectively.

Next, we consider the migration of the oxygen vacancies. For the cubic and rhombohedral LSGMs, only one vacancy migration pathway was considered, while for the orthorhombic and monoclinic LSGMs, two vacancy migration pathways, O_1–O_2 and O_2–O_2, were calculated. Due to their larger distance (beyond 3.9 Å), the migration between the two O_1 sites is extremely unlikely to occur[26] and hence was not considered.

The transition states (TSs) were searched by using the complete LST/QST method. First, the linear synchronous transit (LST) maximization was performed, followed by an energy minimization in directions conjugating to the reaction pathway. The approximated TSs were used to perform quadratic synchronous transit (QST) maximization. From that point, another conjugate gradient minimization was performed. The cycle was repeated until a stationary point was located. In this way the TS can be searched, from which the energy barrier of migration can also be obtained immediately.

For oxygen migration between two equivalent O sites in the C-LSGM and R-LSGM and between two neighbouring O_2 sites, or between the O_1 and O_2 sites in O-LSGM and M-LSGM, it was found that the lowest energy pathway was all curved as shown in Fig. 4, away from the octahedral edge, as has been found previously for oxygen migration in cubic $LaGaO_3$ and other perovskite oxides.[21−23,26,40] Neutron scattering and diffraction studies[10,41,42] have provided evidence for our theoretical results.

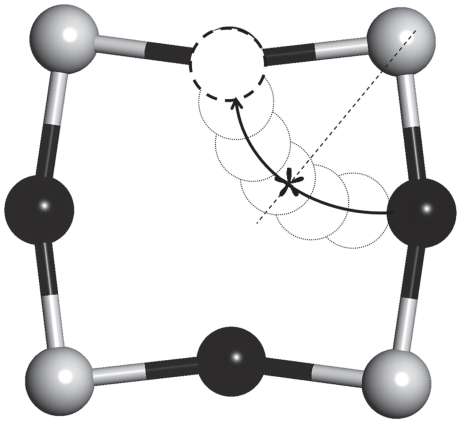


Fig. 4. Schematic representation of the calculated pathway (curved line) of oxygen ion migration between occupied and vacant O_2 sites in O-LSGM. The position of the saddle point is shown with a $*$ note. The white spheres represent Ga/Mg ions, and the black spheres represent O ions.

The calculated oxygen vacancy migration energy E_m along the migration pathway for each structure is shown in Fig. 5. It shows clearly that the migration energy in the C-LSGM is much lower than those of the other three structures. The migration energies increase in the order of $E_m^C \ll E_m^R < E_m^O < E_m^M$ (E_m^O and E_m^M were averaged migration energies

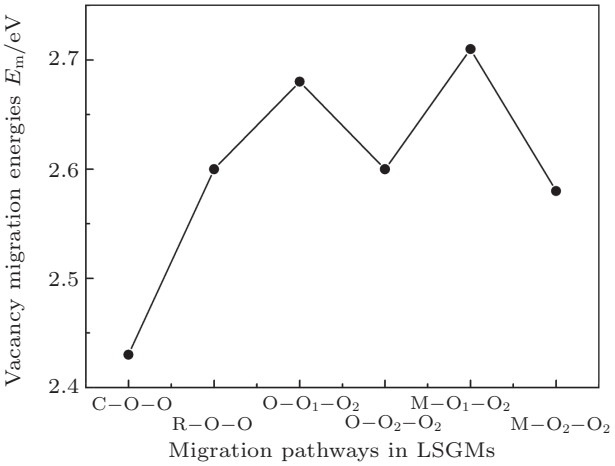


Fig. 5. The calculated vacancy migration energies (E_m) of LSGMs along different migration pathways. C–O–O and R–O–O correspond to the migration pathways of oxygen vacancy between two neighbouring oxygen sites in cubic and rhombohedral LSGMs, respectively. O–O_1–O_2, O–O_2–O_2, M–O_1–O_2, and M–O_2–O_2 correspond to the migration pathways of oxygen vacancy between neighbouring O_1 and O_2 sites or two O_2 sites in orthorhombic and monoclinic LSGMs, respectively.

along O_1–O_2 and O_2–O_2). There is a clear trend towards higher migration energies as the lattice becomes

more distorted (lower symmetry), which is in agreement with other reported perovskite materials.[22,27] Besides, in the O-LSGM and M-LSGM, the migration energies along the pathway linking two O_2 sites are obviously lower than those along the pathway linking the O_1 and O_2 sites. This indicates that the oxygen vacancies can be more easily activated to migrate along the O_2–O_2 than along the O_1–O_2 pathways, and at lower temperatures the former migration pathways are probably in operation alone.

In order to understand the difference between the oxygen vacancy migration energies of the four crystal structures of LSGM, we further counted the number of neighbouring atoms within a spherical region with a radius of 3.2 Å from the migrating oxygen ions and the corresponding average bond lengths at the calculated transition states for LSGMs with various symmetries. The numbers of neighboring atoms are similar for the four structures. Figure 6 shows the relations of the vacancy migration energies and average bond lengths between the migrating oxygen ion and its neighbouring atoms for LSGMs with various symmetries (for O-LSGM and M-LSGM, migration pathways of O_1–O_2 and O_2–O_2 are considered separately). It is found that the migration energy increases when the average bond length of the migrating ion from its neighbouring atoms decreases. The smaller bond length may give rise to the stronger Columbic interactions between the migration oxygen ion and the neighbouring atoms, leading to a larger migration barrier or migration energy of the oxygen vacancy.

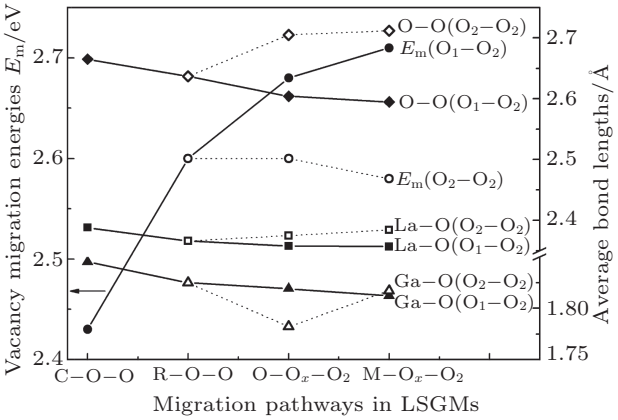


Fig. 6. Average bond lengths between migrating oxygen ions and neighbouring atoms, and the calculated vacancy migration energies (E_m) of LSGMs along different migration pathways (O–O for C-LSGM and R-LSGM, and O_1–O_2 and O_2–O_2 for O-LSGM and M-LSGM). La–O, Ga–O, and O–O are the bonds of La/Sr–O, Ga/Mg–O, and O–O, respectively.

The much lower formation and migration energies of oxygen vacancies in C-LSGM than in the other three structures imply the best oxygen ion conductivity of C-LSGM among the four crystal structures. The oxygen ion conductivity increases in the order of $\sigma_M \leq \sigma_O \leq \sigma_R \ll \sigma_C$, i.e., there is a clear trend towards higher electrical conductivity as the lattice becomes closer to the ideal cubic symmetry.

5. Interpretation of experimental conductivity

In a recent experiment,[8] we found that the LSGM prepared by laser rapid solidification (LRS) exhibited a drastic enhancement in ionic conductivity at high temperatures with respect to that prepared by the high-temperature solid state reaction (SSR2), though both are pure and have similar relative densities. The crystal structures of the SSR2 and the LRS were later identified to be monoclinic with space group $I2/a$, and orthorhombic symmetry with space group *Imma*, respectively, by combining the phonon mode calculations and the Raman spectroscopy.[19] According to the studies by Lerch *et al* and Slater, the orthorhombic LSGM with space group *Imma* at room temperature changes to the cubic symmetry with space group $Pm\bar{3}m$ above 1073 K,[10] while the monoclinic LSGM with space group$I2/a$ at room temperature transforms to rhombohedral symmetry with space group $R3c$ between 723 K and 1273 K.[12] According to the calculated migration energies shown in Fig. 6, the rapid increase in the electrical conductivity of the orthorhombic LSGM at higher temperatures can now be explained by the conspicuous decrease of the migration energy after a phase transition to the cubic LSGM, while the very slow increase in the electrical conductivity of the monoclinic LSGM at higher temperatures can be interpreted by the similar migration energy between the rhombohedral LSGM and its low temperature monoclinic counterpart.

Taking the phase transitions at high temperatures into account, we can infer from the calculated oxygen vacancy formation and migration energies of LSGMs with different symmetries that the cubic and orthorhombic LSGMs are better oxygen ionic conductors than the monoclinic and rhombohedral ones for solid oxide fuel cell applications.

6. Conclusion

First-principles calculations have been employed to investigate oxygen vacancy formation and migra-

tion in cubic, rhombohedral, orthorhombic, and monoclinic $La_{0.9}Sr_{0.1}Ga_{0.8}Mg_{0.2}O_{3-\delta}$ to reveal the underlying mechanism for the abnormal electrical properties of the material at high temperatures. The following points have emerged from our results.

(i) The calculations reveal that C-LSGM has a smaller band gap and much lower vacancy formation and migration energies than R-LSGM, O-LSGM, and M-LSGM, whose band gaps and vacancy formation and migration energies are much larger and of similar values.

(ii) The calculated averaged migration energies increase in the order of $E_{\rm m}^{\rm C} \ll E_{\rm m}^{\rm R} < E_{\rm m}^{\rm O} < E_{\rm m}^{M}$. There is a clear trend towards higher migration energies as the perovskite lattice becomes more distorted. In the O-LSGM and M-LSGM, the migration energies along the pathway linking the two O_2 sites are obviously lower than those along the pathway linking the O_1 and O_2 sites. This indicates that the oxygen vacancies may be more easily activated to migrate along the O_2–O_2 than along the O_1–O_2 pathways in O- or M-LSGM.

(iii) The much lower formation and migration energies of oxygen vacancies in C-LSGM than in the other three structures imply the best oxygen ion conductivity of C-LSGM among the four crystal structures. The oxygen ion conductivity increases as the lattice becomes closer to the ideal cubic symmetry.

(iv) The experimentally observed rapid increase in the electrical conductivity of the orthorhombic LSGM at higher temperatures can be explained by the conspicuous decrease of the migration barriers after a phase transition to the cubic phase. Due to the similar migration energies of the monoclinic and rhombohedral LSGMs, it is not possible for the monoclinic LSGM to exhibit a dramatic increase in electrical conductivity at higher temperatures.

References

[1] Cook R L and Sammells A F 1991 *Solid State Ionics* **45** 311

[2] Mizusaki J 1992 *Solid State Ionics* **52** 79

[3] Kendall K R, Navas C, Thomas J K and Loye H C 1995 *Solid State Ionics* **82** 215

[4] Ishihara T, Matsuda H and Takita Y 1994 *J. Am. Chem. Soc.* **116** 3801

[5] Ishihara T, Kilner J A, Honda M and Takita Y 1997 *J. Am. Chem. Soc.* **119** 2747

[6] Kim J H and Yoo H I 2001 *Solid State Ionics* **140** 105

[7] Rambabu B, Ghosh S, Zhao W C and Jena H 2006 *J. Power Sources* **159** 21

[8] Zhang J, Liang E J and Zhang X H 2010 *J. Power Sources* **195** 6758

[9] Drennan J, Zelizko V, Hay D, Ciacchi F T, Rajendran S and Badwal S P S 1997 *J. Mater. Chem.* **7** 79

[10] Lerch M, Boysen H and Hansen T 2001 *J. Phys. Chem. Solids* **62** 445

[11] Vasylechko L, Vashook V, Savytskii D, Senyshyn A, Niewa R, Knapp M, Ullmann H, Berkowski M, Matkovskii A and Bismayerg U 2003 *J. Solid State Chem.* **172** 396

[12] Slater P R, Irvine J T S, Ishihara T and Takita Y 1998 *J. Solid State Chem.* **139** 135

[13] Gong W Q, Gopalan S and Pal U B 2006 *J. Power Sources* **160** 305

[14] Fukui T, Ohara S, Murata K, Yoshida H, Miura K and Inagaki T 2002 *J. Power Sources* **106** 142

[15] Yoo J S, Lee S, Yu J H, Woo S K, Park H and Kim H G 2009 *J. Power Sources* **193** 593

[16] Zhai Y L, Ye C, Xiao J Z and Dai L 2006 *J. Power Sources* **16** 316

[17] Feng M and Goodenough J B 1994 *Eur. J. Solid State Inorg. Chem.* **31** 663

[18] Trofimenko N and Ullmann H 1999 *Solid State Ionics* **118** 215

[19] Zhang J, Liang E J, Wang Y F and Jia Y *The Journal of Light Scattering* **23** 357

[20] Akihide K and Isao T 2004 *J. Phys. Chem.* B **108** 9168

[21] Islam M S 2002 *Solid State Ionics* **154–155** 75

[22] Islam M S 2000 *J. Mater. Chem.* **10** 1027

[23] Khan M S, Islam M S and Bates D R 1998 *J. Phys. Chem.* B **102** 3099

[24] Lei X L, Zhu H J, Wang X M and Luo Y H 2008 *Chin. Phys.* B **17** 3687

[25] Chen Q and Cao H H 2004 *Chin. Phys.* **13** 2121

[26] Jones A and Islam M S 2008 *J. Phys. Chem.* C **112** 4455

[27] De Souza R A, Islam M S and Ivers-Tiffée E 1999 *J. Mater. Chem.* **9** 1621

[28] Zhang J H, Ding J W and Lu Z H 2009 *Acta Phys. Sin.* **58** 1901 (in Chinese)

[29] Tang C, Tuttle B and Ramprasad R 2007 *Phys. Rev.* B **76** 073306

[30] Nolan M, Fearon J E and Watson G W 2006 *Solid State Ionics* **177** 3069

[31] Tan X Y, Chen C L and Jin K X 2011 *Acta Phys. Sin.* **60** 107105 (in Chinese)

[32] Yi Y, Ding Z J, Li K, Tang Y J and Luo J S 2011 *Acta Phys. Sin.* **60** 097503 (in Chinese)

[33] Yi Y, Li K, Ding Z J, Yi Z, Luo J S and Tang Y J 2011 *Acta Phys. Sin.* **60** 107502 (in Chinese)

[34] Ji Z H, Zeng X H, Cen J P and Tan M Q 2010 *Acta Phys. Sin.* **59** 1219 (in Chinese)

[35] Delley B 1990 *J. Chem. Phys.* **92** 508

[36] Delley B 1996 *J. Phys. Chem.* **100** 6107

[37] Perdew J P, Burke K and Ernzerhof M 1996 *Phys. Rev. Lett.* **77** 3865

[38] Bellaiche L and Vanderbilt D 2000 *Phys. Rev.* B **61** 7877

[39] Liu J C, Zhang X M, Chen M A, Tang J G and Liu S D 2010 *Acta Phys. Sin.* **59** 5641 (in Chinese)

[40] Mather G C and Islam M S 2005 *Chem. Mater.* **17** 1736

[41] Günter M M, Boysen H, Corte C, Lerch M and Suard E 2005 *Z. Kristallogr.* **220** 218

[42] Yashima M, Nomura K, Kageyama H, Miyazaki Y, Chitose N and Adachi K 2003 *Chem. Phys. Lett.* **380** 391